Multiferroic phases of $Eu_{1-x}Y_xMnO_3$

J. Hemberger,[1] F. Schrettle,[1] A. Pimenov,[1] P. Lunkenheimer,[1] V. Yu. Ivanov,[2] A. A. Mukhin,[2] A. M. Balbashov,[3] and A. Loidl[1]

[1]*Experimentalphysik V, Center for Electronic Correlations and Magnetism, University of Augsburg, D-86135 Augsburg, Germany*

[2]*General Physics Institute of the Russian Academy of Sciences, 38 Vavilov Street, 119991 Moscow, Russia*

[3]*Moscow Power Engineering Institute, 14 Krasnokasarmennaja Street, 111250 Moscow, Russia*

(Received 9 March 2006; revised manuscript received 9 November 2006; published 16 January 2007)

We report on structural, magnetic, dielectric, and thermodynamic properties of $Eu_{1-x}Y_xMnO_3$ for Y doping levels $0 \leqslant x < 1$. This system resembles the multiferroic perovskite manganites $RMnO_3$ (with R=Gd, Dy, Tb) but without the interference of magnetic contributions of the $4f$ ions. In addition, it offers the possibility to continuously tune the influence of the A-site ionic radii. For small concentrations $x \leqslant 0.1$ we find a canted antiferromagnetic and paraelectric ground state. For higher concentrations $x \geqslant 0.3$ ferroelectric polarization coexists with the features of a presumably spiral magnetic phase analogous to the observations in $TbMnO_3$. In the intermediate concentration range around $x \approx 0.2$ a multiferroic scenario is realized combining weak ferroelectricity and weak ferromagnetism, presumably due to a conelike magnetic structure.

DOI: 10.1103/PhysRevB.75.035118 PACS number(s): 77.22.Ch, 77.22.Ej, 75.30.Kz, 75.50.Ee

I. INTRODUCTION

In recent years multiferroics have attracted an increasing scientific and technological interest in the large community working on functional transition-metal compounds.[1] Within this rare class of materials magnetic order coexists with long-range polar order and both order parameters are strongly coupled. Prominent examples for such multiferroics may be found among Cr-based spinels,[2,3] the kagomé staircase compound $Ni_3V_2O_8$,[4] rare-earth manganites such as hexagonal $YMnO_3$ and $HoMnO_3$,[5,6] orthorhombic $TbMn_2O_5$,[7] or finally, perovskites such as $TbMnO_3$.[8]

In this latter class of heavy rare-earth compounds $RMnO_3$ (R=Gd, Tb, Dy) (Refs. 9 and 10) finite ferroelectric polarization is induced due to the partial frustration and corresponding long-range modulation of the magnetic structure. The importance of the Dzyaloshinskii-Moriya interaction for the occurrence of ferroelectricity in noncollinear magnets has been pointed out recently.[11–13] Starting from the lanthanide manganite with the perovskite tolerance factor close to unity, the substitution of La at the A sites by rare-earth elements with smaller ionic radii (from Pr to Ho) leads to a successive increase of the orthorhombic distortion, accompanied by a decrease of the Mn-O-Mn bond angles and an increase of the buckling and tilting angles of the MnO_6 octahedra, respectively.[8,9] Equivalent results can be obtained when continuously replacing La^{3+} by smaller ions like in $La_{1-y}Gd_yMnO_3$.[14] The enhanced tilting of the MnO_6 octahedra leads to an increasing importance of antiferromagnetic (AFM) next-nearest neighbor interactions competing with the nearest neighbor superexchange within the ferromagnetic (FM) ab-planes of the A-type AFM structure. This weakening of the effective magnetic interaction promotes a tendency towards frustration and complex spin states.[15] Hence, the transition temperature into the A-type AFM phase is not only reduced, but for the heavy rare-earth compounds with smaller ionic radii a long-wavelength incommensurate magnetic structure is established for temperatures below $T_N \approx 50$ K.[14–16] Recent studies showed, that for the case of $TbMnO_3$ the long wavelength AFM structure remains incommensurate but experiences a change from a longitudinally modulated sinusoidal structure to a magnetically transverse spiral and ferroelectric structure for $T < 28$ K.[17] In this spiral magnetic phase magnetoelectric coupling via long-range modulation of the magnetic structure leads to the loss of inversion symmetry and the onset of ferroelectric polarization.[17] The onset of ferroelectricity is connected with the change of the magnetic structure from a collinear to a noncollinear modulation[17,18] and independent of the commensurability of the spin sector. For $TbMnO_3$ it was even shown that in magnetic fields along the b axis a change from an incommensurate to a commensurate spin structure can be driven, which is accompanied by a reorientation of the ferroelectric polarization from c to a.[19,20] Very recently excitations of the multiferroic state have been observed experimentally,[21] and have also been described theoretically.[22]

The existence of a ferroelectric lattice distortion is especially remarkable due to the fact that these compounds possess a quite robust Jahn-Teller- (JT-) type orbital order, which sets in at temperatures well above 1000 K. From a principal point of view Jahn-Teller active orbital degrees of freedom are the "natural enemy" of off-center ferroelectric distortions.[23] Undistorted orbital electron-density distributions are point symmetric carrying no electric dipole moment. Hence, if the lattice is able to relax into a lower symmetry via a Jahn-Teller distortion this transition is expected not to be dipolar. In this sense the ferroelectricity in the heavy rare-earth manganites exists not due to, but despite the superimposed orbital order and comparing the relevant energy scales it has to be regarded as a second-order effect. Therefore the ferroelectric distortion is rather weak and so far could not be proven directly using high-resolution neutron or x-ray diffraction techniques. However, the onset of ferroelectricity was documented via pyroelectric measurements and is connected to a distinct anomaly in the real part of the dielectric permittivity[10] and clear features in the anisotropic thermal expansion.[24] This underlines that the ferroelectric distortions are driven by frustrated magnetic interactions via local exchange striction.[8]

Within the scenario of partially frustrated Mn spins the role of the magnetic *A* sites is not completely clear so far. Generally, the moments of the rare-earth ions are polarized due to the coupling with the Mn subsystem resulting in a noticeable anisotropic contribution to the low-temperature magnetic and thermodynamic properties of the manganites as, e.g., recently studied in detail for the systems $PrMnO_3$ and $NdMnO_3$.[25] For Gd, Tb, and Dy at the ordering temperature of the rare-earth moments significant anomalies in the dielectric constant can be found denoting the possible influence of the magnetic *A* sites.[10] High-resolution synchrotron x-ray-diffraction experiments yield evidence that in the case of $DyMnO_3$ besides a strong magnetic coupling between rare earth and Mn ions a strong interference of Mn- and Dy-induced structural distortions has to be considered.[26]

In this paper we report structural, magnetic susceptibility, magnetization, and specific-heat measurements for single and polycrystalline $Eu_{1-x}Y_xMnO_3$. Our focus is directed towards the isovalent doping of the trivalent *A* site in $RMnO_3$, with *R* denoting elements Eu^{3+} ($4f^3$) or Y^{3+} ([Kr]).[27] This allows for a systematic variation of the ionic radii and possibly of the Mn-O-Mn angle, which we relate to the development of the complex magnetic ground states and ferroelectric phases analogous to the pure rare-earth compounds $RMnO_3$ with R=Gd,Dy,Tb. The system (Eu:Y)MnO_3 offers the possibility to *continuously* control the *A*-site volume of the orbitally ordered perovskite structure and thus to tune the corresponding multiferroic phases without the additional influence of a magnetic rare-earth moment. A further aspect of the system $Eu_{1-x}Y_xMnO_3$ is the robustness of long-range polar order against the influence of purely structural *A*-site disorder.

II. EXPERIMENTAL DETAILS

$Eu_{1-x}Y_xMnO_3$ single crystals were grown in Ar flow by a floating-zone method with radiation heating for Y concentrations x=0, 0.1, 0.2, 0.3, and 0.5 (for the details of the crystal growth see Ref. 28). The specimens used in this study were cuboids cut from larger crystals and had typical dimensions $2\times1.5\times1$ mm^3 along the *a*, *b*, and *c* direction (*Pbnm* setting), respectively. Additional concentrations have been prepared as polycrystals for higher concentrations up to x =0.95 using conventional solid-state reaction methods.[28] Powder-diffraction experiments were performed on powder of crushed single and polycrystals at room temperature with a STOE diffractometer utilizing Cu K_α radiation with a wavelength λ=0.1541 nm. The magnetic susceptibility and the magnetization were recorded using a commercial SQUID magnetometer for temperatures $T<400$ K and external magnetic fields up to 50 kOe. The dielectric constant has been measured employing a frequency-response analyzer (Novocontrol Alpha Analyzer and HP4284A) and the spontaneous electric polarization was recorded as an integrated pyrocurrent. The specific heat was measured in a PPMS system (Quantum Design).

III. RESULTS AND DISCUSSION

A. Structure

A typical result for the structural characterization of the samples by x-ray diffraction is shown in Fig. 1. The diffraction patterns were refined using Rietveld analysis. All samples investigated revealed the O′ orthorhombic structure (*Pbnm*). No impurity phases were detected above background level for Y concentrations $x<0.75$. For higher concentrations (as denoted in Fig. 2), small traces of the hexagonal ($P63cm$) phase of $YMnO_3$ show up, which could be estimated to be below 2% and will not considerably influence the regarded macroscopic properties. The lattice constants and the volume of the unit cell as derived from the profile analysis are shown in Fig. 2. In addition, the data for the system $La_{1-y}Gd_yMnO_3$, which was taken from Ref. 14, is displayed on a separate scale. Both scales, for Gd-doping *y* and Y-doping *x* are shifted to achieve an overlap of the structural data. For all concentrations we find $b>a>c/\sqrt{2}$ indicative for a static JT distortion superimposed on the high-

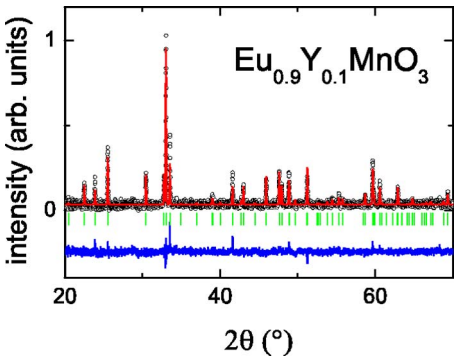

FIG. 1. (Color online) Representative powder XRD Pattern for the $Eu_{0.9}Y_{0.1}MnO_3$. The lines show the results of a Rietveld refinement (upper line through the data points) and the corresponding deviation from the experimental data (below the data). The bars in between denote allowed reflections of the *Pbnm* structure.

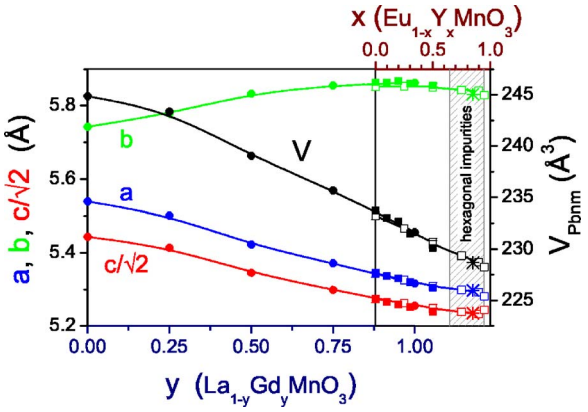

FIG. 2. (Color online) Lattice constants *a*, *b*, and $c/\sqrt{2}$ (left scale) and volume of the unit cell (right scale) in $Eu_{1-x}Y_xMnO_3$ and $La_{1-y}Gd_yMnO_3$ vs concentration of Y (*x*, upper scale, squares) and Gd (*y*, lower scale, circles). Both scales are shifted to adapt the overlap of the data. The solid symbols represent data evaluated from regrinded single crystals, the open symbols represent data evaluated from polycrystalline material. The asterisks denote the lattice parameters of pure $TbMnO_3$, which are placed to match the values of $Eu_{1-x}Y_xMnO_3$ close to $x\approx0.85$. Within the hatched area small traces of hexagonal impurity phases (<2%) have been detected.

temperature O-type (i.e., not JT distorted) orthorhombic structure, which results from the buckling and tilting of the MnO_6 octahedra due to geometrical constraints. However, for $Eu_{1-x}Y_xMnO_3$, despite the continuous shrinking of the lattice volume V, the orthorhombic distortion parametrized by $\varepsilon=(b-a)/(a+b)$ tends to saturate for higher Y-concentrations. The inequality of the lattice constants a and b reflects the tilting of the octahedra around the b axis and implies significant deviations from 180° of the Mn-O-Mn bond angle ϕ within the ab plane. Another quantity reflecting the development of ϕ is the tilting distortion along b of the A site as obtained from the Rietveld refinement of the atomic positions. This parameter (not shown) is almost constant for the system $Eu_{1-x}Y_xMnO_3$ in contrast to the less distorted system $La_{1-y}Gd_yMnO_3$.[14] This implies that the alteration of the spin system due to the influence of the Mn-O-Mn bond angle may not be the only valid mechanism for $Eu_{1-x}Y_xMnO_3$. In addition, the variation of the magnetic exchange via the reduction of the volume and the corresponding changes in the orbital overlap may also have to be considered. Also the A-site disorder and the corresponding variance in the A-site ionic radii could play an important role. The asterisks in Fig. 2 display the structural parameters of pure $TbMnO_3$.[16] The data agree with the findings for the Y concentration $x\approx0.85$. If only taking into account the averaged ionic radii, the values of the Tb system should be located at $x\approx0.4$.[29] For the system $GdMnO_3$ the equivalent concentration is $x\approx0.3$, while the value is expected to be close to $x\approx0.15$. This shows that for $Eu_{1-x}Y_xMnO_3$ the lattice is less contracted than expected when compared to the pure rare-earth manganites.

B. Magnetism

Figure 3 shows the magnetic dc susceptibilities $\chi=M/H$ for concentrations $x\leqslant0.5$. At elevated temperatures all susceptibilities follow a Curie-Weiss (CW) law as revealed by the inverse representation in the lower frame of Fig. 3. The corresponding effective paramagnetic moments p_{eff} are plotted in the lower inset of Fig. 3. p_{eff} is decreasing due to the decreasing rare-earth contribution. Y^{3+} is nonmagnetic and for Eu^{3+} the $4f^6$ configuration leads to $J=0$. However, for Eu low-lying multiplets give rise to a Van-Vleck type of contribution, which in this temperature regime is nearly Curie type and thus enhances the effective paramagnetic moment. For a more detailed analysis the paramagnetic high temperature behavior was fitted by a sum of the contribution of Eu^{3+} $[\propto(1-x)]$ and the CW-type contribution of Mn^{3+}. For the Eu contribution we used the well-known free-ion susceptibility of Eu^{3+} determined by its excited multiplets with $E_1\approx500$ K and $E_2\approx3E_1$ for $J=1$ and $J=2$, respectively.[30,31] At high temperatures it is linear in $1/T$ while at low T it is determined by a temperature-independent Van-Vleck contribution. All our data can be nicely described using $p_{\mathrm{eff,Mn}}$ as plotted in the lower inset of Fig. 3 (○). The manganese contribution turns out to be independent of x and agrees well with the expected theoretical value $2\mu_B\sqrt{[S(S+1)]}=4.9\mu_B$. For concentrations $x\leqslant0.5$ the CW temperatures of the Mn subsystem are $\Theta\approx-58\pm4$ K and are almost independent of x. This result is in agreement with corresponding findings in $La_{1-y}Gd_yMnO_3$ for high Gd concentrations.[14]

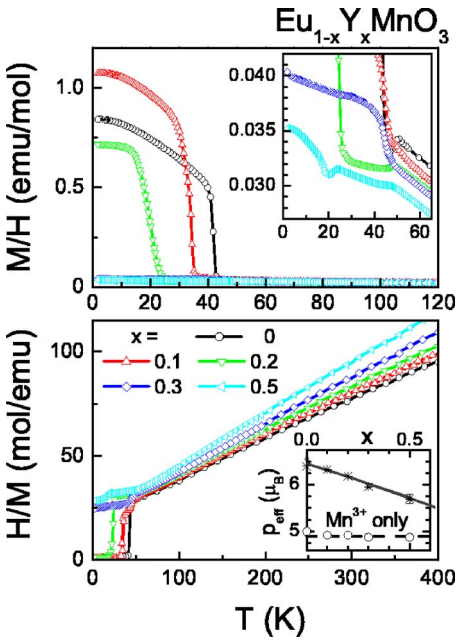

FIG. 3. (Color online) Temperature dependence of the magnetic dc susceptibility $\chi=M/H$ (upper frame, for $T<100$ K) and the inverse dc susceptibility $1/\chi=H/M$ (lower frame, for $T<400$ K) for various concentrations of $Eu_{1-x}Y_xMnO_3$ as measured along c in an external magnetic field of 1 kOe. The upper inset provides an expanded view of M/H close to the magnetic phase transitions. The lower inset shows the effective paramagnetic moment p_{eff} as obtained from a simple Curie-Weiss-type evaluation (∗) of the linear regime of $1/\chi$ above $T=100$ K and from an analysis separating the contributions of Eu and Mn as described in the text (○).

Below 50 K all compositions undergo a magnetic transition. This transition was clearly detected by heat-capacity experiments, which will be discussed later. It can only be seen as a small change of slope in the temperature dependence of the magnetic susceptibility, as it is not connected with the onset of a ferromagnetic component (see the upper inset of Fig. 3). For all compounds a second, much stronger anomaly can be detected in the magnetic susceptibility between 20 and 40 K. For $x=0$, 0.1, and 0.2 the appearance of spontaneous magnetization signals weak ferromagnetism. This is demonstrated in the upper frame of Fig. 3, which shows a strong upturn of magnetization indicating a significant ferromagnetic contribution. This FM component arises due to spin canting, which can be explained by the Dzyaloshinsky-Moriya interaction and is an intrinsic feature of the CAFM state in $RMnO_3$ systems.[32,33] For $x=0$, pure $EuMnO_3$, it is known that the two subsequent magnetic phase transitions are from the paramagnetic into an incommensurate AFM structure and subsequently into the canted A-type spin structure (CAFM).[9] Based on our dielectric results we believe that the same is true for $x=0.1$, but that for higher concentration $0.1<x<0.3$ the low-temperature anomalies correspond to a transition into a new, weakly ferromagnetic phase, which in addition is ferroelectric (AFM-3, see later). As stated above, T_{CAFM} continuously decreases

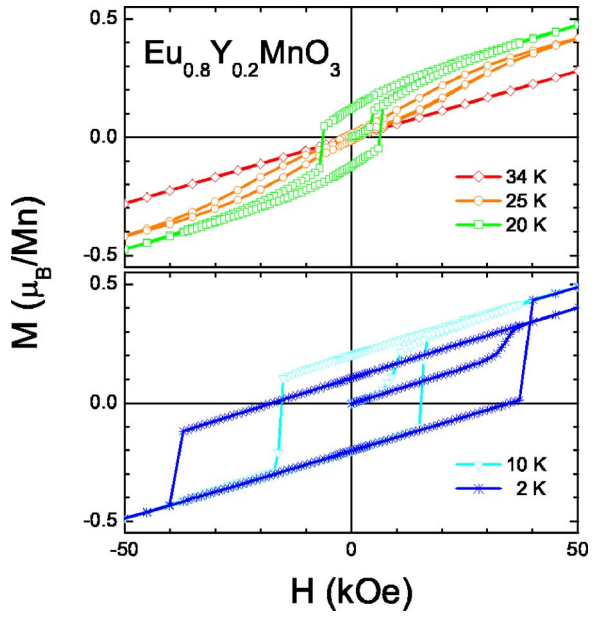

FIG. 4. (Color online) Magnetization along c in $Eu_{0.8}Y_{0.2}MnO_3$ as a function of the external magnetic field for a series of temperatures between 2 and 34 K.

from 140 K in $LaMnO_3$ down to about 20 K in $GdMnO_3$. For the system $Eu_{1-x}Y_xMnO_3$ this transition is shifted to $T \approx 0$ for Y concentrations of about 0.2. For $TbMnO_3$ and for concentrations $x \geqslant 0.2$ in $Eu_{1-x}Y_xMnO_3$ no weak ferromagnetism can be found. In $TbMnO_3$ the character of the magnetic phase changes from a sinusoidal to a helicoidal (spiral) magnetic structure at $T \approx 27$ K, which is in addition connected to the onset of ferroelectricity.[17] In $Eu_{1-x}Y_xMnO_3$ for $x \geqslant 0.3$ in the temperature range between 20 and 30 K a magnetic transition between two antiferromagnetic phases (AFM-1, AFM-2) without any ferromagnetic component can be detected. As discussed later this transition from AFM-1 to AFM-2 is as well connected with the onset of ferroelectricity. In analogy to the pure $TbMnO_3$ these two magnetic structures probably are collinear sinusoidal and a spiral (noncollinear) at low temperatures. A spiral spin configuration is essential for the onset of ferroelectricity.[11,12,18] It should be noted that at least for the composition $x=0.5$ additional small anomalies can be found at the ferroelectric transitions at 24 and 18 K, indicative for a partial rearrangement of the magnetic structure.

Figure 4 shows the magnetization $M(H)$ for $Eu_{0.8}Y_{0.2}MnO_3$ in magnetic fields up to 5 T as measured after zero-field cooling. At $T=34$ K (upper frame of Fig. 4) an apparently paramagnetic magnetization behavior is detected, albeit the sample at this temperature is already magnetically ordered as can be deduced from the specific-heat data (presented below). At 25 K the CAFM state can be induced by the magnetic field as reflected by the twofold hysteresis loop with the typical signature of a smeared-out metamagnetic phase transition at $H \approx 30$ kOe. On further decreasing temperature this metamagnetic transition becomes fully irreversible and the two loops are merged into one as it is characteristic for a weak ferromagnet. After the initial increase of the field the CAFM state persists and only the ferromagnetic component is switched at a sharply defined coercive field, which increases up to $H_c \approx 40$ kOe for the lowest temperatures. At 2 K (lower frame of Fig. 4) even an intermediate state with a smaller ferromagnetic component is stabilized after the initial increase of the magnetic field leading to an asymmetric shape of the hysteresis loop.

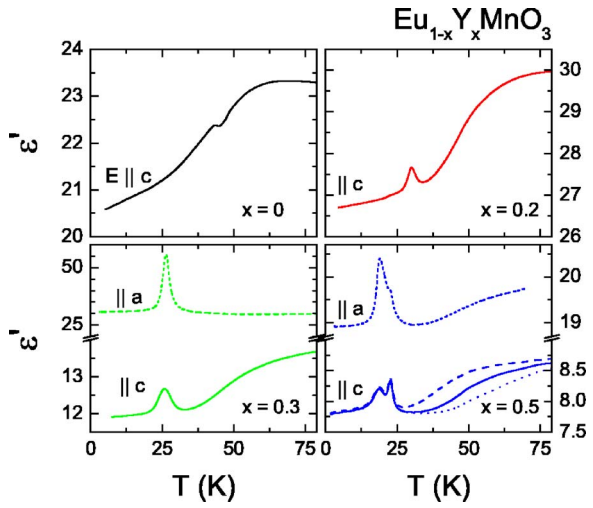

FIG. 5. (Color online) Temperature dependence of the real part of the permittivity ε' for the Y concentrations $x=0$, 0.2, 0.3, and 0.5 as measured at $\nu=100$ kHz. The lower right frame ($x=0.5$) shows additional data for the frequencies 27 kHz (dashed) and 250 kHz (dotted). Additional data for $E \| a$ is given for the concentrations $x=0.3$ and 0.5 (lower frames, short dashes). In general, the measured data of ε' may comprise a constant additional contribution due to stray capacitance of the measurement setup together with a relative uncertainty of up to 25% due to the determination of the sample geometry. Hence, the absolute values of $\varepsilon'(T)$ are not discussed. However, the relative accuracy of the measurement is much higher and lies within the thickness of the lines.

C. Dielectric properties

Figure 5 displays the real part of the dielectric constant as measured in the radio-frequency range for various concentrations of $Eu_{1-x}Y_xMnO_3$. All $\varepsilon'(T)$ curves show a steplike increase with increasing temperature along the c direction. Its point of inflection is located around 50 K but as shown exemplarily for the concentration $x=0.5$ (the lower right frame of Fig. 5) its position is strongly frequency dependent. Similar phenomena have already been found, e.g., for $TbMnO_3$ and have been ascribed to the relaxation of localized polarons.[8] In the following we will concentrate on the anomalies below 45 K. For pure $EuMnO_3$ only a tiny kink can be found near $T \approx 43$ K. This coincides with the onset of weak ferromagnetism in the CAFM phase as revealed from the magnetic susceptibility measurements. For $x=0.2$ a prominent peak occurs at the transition into the magnetically ordered (AFM-2) and ferroelectric phase near $T_{\text{AFM-2}} \approx 30$ K. A second anomaly can exist at $T_{\text{AFM-3}} \approx 22$ K, but this feature is much weaker and can hardly be recognized. At this latter transition the ferroelectric order persists but the magnetic structure is altered and a weak ferromagnetic com-

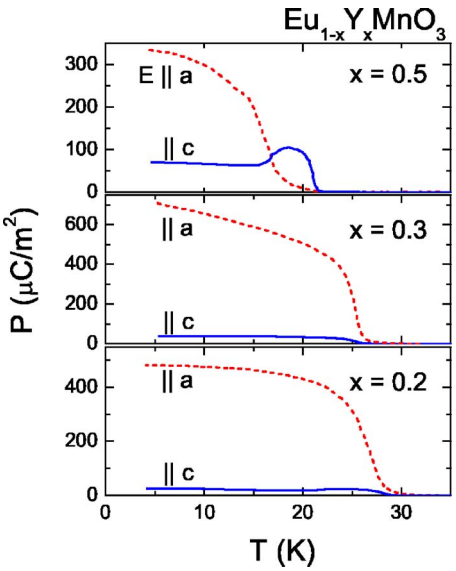

FIG. 6. (Color online) Electric polarization as measured on heating after cooling down in a poling field of about 100 V/mm for the Y concentrations $x=0.2$, 0.3, and 0.5.

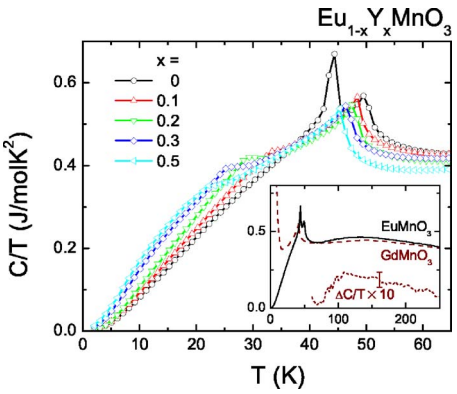

FIG. 7. (Color online) Heat capacity of $Eu_{1-x}Y_xMnO_3$ plotted as C/T as a function of temperature. The inset compares the data for pure $EuMuO_3$ (solid line) and $GdMnO_3$ (dashed line) for temperatures up to 250 K. The dotted line represents the difference multiplied by a factor of 10.

ponent sets in. For $x=0.3$ a pronounced dielectric anomaly is located at the antiferromagnetic and ferroelectric transition at $T_{\text{AFM-2}} \approx 26$ K and, finally, for $x=0.5$ it forms a double-peak structure at roughly 23 and 19 K. A similar double-structured peak can also be detected along the a direction, however with shifted weight from the higher to the lower temperature peak. These anomalies in $\varepsilon'(T)$ coincide with the onset of ferroelectricity as will be described later. For the concentrations $x=0.2$, 0.3, and 0.5 the electric polarization $P(T)$ is shown in Fig. 6. As revealed by the uppermost frame of Fig. 6, obviously the double structure in $\varepsilon'(T)$ for $Eu_{0.5}Y_{0.5}MnO_3$ (the lower right frame of Fig. 5) corresponds to the partial spontaneous reorientation of P from the c to the a direction. This is in accord with the recent results obtained for $x \approx 0.4$ by Kuwahara and co-workers.[29] Such a spontaneous reorientation of the electric polarization is not reported for the pure systems $RMnO_3$.[10] For the compositions $Eu_{1-x}Y_xMnO_3$ with $x=0.3$ and 0.2 no temperature-dependent reorientation of the polarization could be observed as it is shown in the lower frames of Fig. 6.

Ferroelectricity (FE) does not occur for concentrations below $x<0.2$. Nevertheless, it is remarkable that a canted, i.e., weakly ferromagnetic state and FE are not mutually exclusive. For $x=0.2$ the system first becomes ferroelectric at $T_{\text{FE}} \approx 30$ K and then the ferromagnetism evolves roughly 8 K below. It is remarkable that despite the magnetoelectric origin of the FE order no clear anomaly in $P(T)$ can be observed for $x=0.2$ around 23 K where a spontaneous FM component sets in. However, as can be seen from Fig. 4 the values for the spontaneous magnetization stay below $0.2\mu_B$ per Mn^{3+} ion. This is only 1/20th of the maximal ordered moment of $4\mu_B$. Thus the effective FM moment can be explained by a canting of the presumably spiral magnetic structure of less than 3°, which represents only a small modification of the magnetic structure. The FM and FE order parameters for $x=0.2$ reach values comparable to the neighboring concentrations. This points against a scenario of phase separation where one would expect a reduction of the low-temperature saturation values for P and M according to the corresponding fractions of the ferromagnetic and ferroelectric phases.

In a strict sense, $Eu_{0.8}Y_{0.2}MnO_3$ is the only multiferroic system among the rare-earth perovskite manganites reported so far, where the ground state seems to combine the properties of ferromagnetism and ferroelectricity. The most prominent examples such as $TbMnO_3$ never show a finite spontaneous FM and FE order parameter at the same time.

D. Specific heat

Figure 7 presents the results of heat-capacity measurements in $Eu_{1-x}Y_xMnO_3$ as a function of temperature. The heat capacity, plotted as C/T, is shown for temperatures $T<65$ K and concentrations $0 \leqslant x \leqslant 0.5$. A well-defined lambdalike anomaly shows up between 45 and 50 K for all concentrations under investigation. In agreement with the magnetization data this anomaly has to be interpreted as the onset of magnetic order (AFM-1). The transition temperature is slightly decreasing with increasing Y concentration. Below 45 K for each concentration a further anomaly appears at lower temperatures, which for pure $EuMnO_3$ is characterized by a sharp peak in C/T at 44 K corresponding to the transition into the A-type AFM phase (see Fig. 3). For the Y-doped samples this feature gets considerably smeared out presumably due to the influence of disorder. Again the corresponding transition temperature as denoted by the onset of the broad shoulderlike contribution is monotonously decreasing with increasing x down to about 20 K for $x=0.5$. However, even though the shape of this anomaly in C/T is not altered qualitatively, the corresponding transition refers to different ground states for different compositions. As it was already revealed in Figs. 3 and 6 the onset of spontaneous magnetization corresponds to the transition into a new magnetic ground state with FM and FE components for concentrations $x \approx 0.2$. For higher concentrations no FM component develops down to lowest temperatures. The onset of FE polariza-

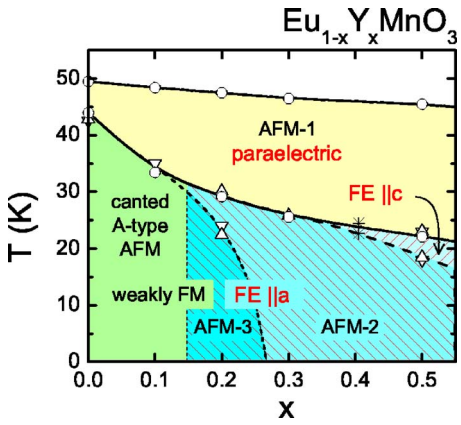

FIG. 8. (Color online) (T,x)-phase diagram of $Eu_{1-x}Y_xMnO_3$ for Y concentrations $0 \leqslant x \leqslant 0.5$. The data points were obtained from the measurements of the specific heat (○), the magnetization (▽), the permittivity (△), and from Ref. 29 (∗). (The attribution of the spiral or collinear nature of the magnetic order was inferred from the comparison with experimental results on other rare-earth compounds and theoretical models from literature as described in the text.)

tion coincides with the change in the magnetic structure from AFM-1 to AFM-2, which presumably corresponds to a change from collinear sinusoidal to a noncollinear spiral magnetism.[17,18] The absence of any qualitative differences in the curvature of C/T for the different compositions reflects that the corresponding ground states together with their partially frustrated spin structures are nearly degenerate.

It is worth mentioning that the low-temperature specific heat in this system differs essentially from that of $GdMnO_3$ or $TbMnO_3$ due to the missing contribution of the magnetic rare earths.[8,14] Neither a Schottky-type contribution as found due to the rare-earth spins, which are polarized in the effective exchange field from the CAFM Mn sublattice, nor an anomaly due to the subsequent ordering of the magnetic rare-earth sublattice in the temperature range below 10 K can be detected for $Eu_{1-x}Y_xMnO_3$. For comparison, the inset of Fig. 7 shows data for pure $GdMnO_3$ and $EuMnO_3$. Besides the mentioned differences at low temperatures for $EuMnO_3$ an additional contribution at higher temperatures is observed. This contribution cannot be explained by the slight differences of the phonon spectrum because Gd and Eu have very similar masses. $\Delta C(T)$ shows a broad peak at around 120 K and can be explained by the relatively small splitting of the Eu multiplet, which also gives rise to the Van-Vleck contribution to the magnetic susceptibility, discussed above.

IV. PHASE DIAGRAM

Based on the results shown above, from the magnetic and dielectric measurements as well as from the heat capacity, a detailed (x,T)-phase diagram can be constructed and is shown in Fig. 8. The paramagnetic regime above $T_N \approx 45-50$ K, is followed by an ordered phase (AFM-1) with presumably sinusoidal collinear AFM structure of the manganese moments, an interpretation guided by the results for the non-FE phases of the pure compounds $EuMnO_3$ and $TbMnO_3$.[8,17,18] For small Y concentrations, $x \leqslant 0.2$ a weakly ferromagnetic phase is established. It is the well-known canted *A*-type antiferromagnet of the pure compound. However, based on theoretical arguments, this collinear structure never can become ferroelectric. Hence we conclude, that for $x=0.2$ a new magnetic phase is established (AFM-3), which is weakly ferromagnetic. We propose that this phase represents a conelike structure, breaking the inversion symmetry allowing for ferroelectricity and carrying a weak ferromagnetic moment. For higher concentrations, $x \geqslant 0.3$, the ground state is antiferromagnetic and ferroelectric without a ferromagnetic component. From theoretical considerations in these perovskitic rare-earth manganites a one-to-one correspondence between the onset of ferroelectricity and a noncollinear spiral AFM structure has to be assumed.[12,17,18] However, it remains unclear so far and it cannot be judged from our experiments, if the magnetic structure of the ferroelectric ground state is incommensurate or if a commensurate long-wavelength magnetic vector is established. In a small regime around $x \approx 0.2$ weak ferromagnetism and weak ferroelectricity coexist in contrast to the pure multiferroic rare-earth manganites.

Regarding the volume of the unit cell, the series $Eu_{1-x}Y_xMnO_3$ covers the values of $GdMnO_3$ and $TbMnO_3$. Pure $EuMnO_3$ is not ferroelectric. Pure $TbMnO_3$ is spontaneously ferroelectric along *c* within a spiral AFM structure.[10] Pure $GdMnO_3$ is ferroelectric along *a* in a weak external magnetic field along *b*, which destroys the *A*-type AFM structure.[10] For $Eu_{1-x}Y_xMnO_3$ a concentration slightly lower than $x=0.2$ probably will reproduce this property of $GdMnO_3$. However, according to Fig. 2 the Eu:Y system corresponding to $GdMnO_3$ should have $x \approx 0.2$. This composition is already ferroelectric without magnetic field. The magnetic structure of this weakly FM and FE phase is not clear, however, a spontaneously canted spiral AFM phase could combine both ferroic properties. However, concerning the volume of the unit cell it could not be reproduced by pure single-crystalline $Eu_{1-x}Y_xMnO_3$ close to $x \approx 0.85$ as shown in Fig. 2. In $TbMnO_3$ there is an additional anisotropy due to Tb ions and Tb-Mn exchange, which could lead to the observed electric polarization along the *c* axis. This should be taken into account for the comparison between $TbMnO_3$ and $Eu_{1-x}Y_xMnO_3$ systems. However, the tendency towards a spontaneous ferroelectric component along *c* is already indicated also for $Eu_{1-x}Y_xMnO_3$ at lower Y concentrations such as $x=0.5$ (Fig. 6).

It is interesting that only the weak FE component along *a* coexists with spontaneous weak ferromagnetism, namely, within the concentration range around $x \approx 0.2$, while for higher concentrations, where at least an intermediate FE component along *c* is detected, no weak ferromagnetism shows up. According to the symmetry properties of the magnetoelectric coupling for the rare-earth manganites,[12,17,18] the ferroelectric polarization vector is orthogonal to both, the vector of the magnetic spiral and the magnetic modulation vector, which points along the *b* axis.[9] For $TbMnO_3$ (Ref. 17) and analog for the higher Y concentrations of $Eu_{1-x}Y_xMnO_3$ the ferroelectric component points along the *c* direction, which is compatible with a spiral vector along *a* (i.e., the spins rotating in the *bc* plane). For $GdMnO_3$ (in

small magnetic fields along b[24]) and similarly for the concentrations around $x \approx 0.2$ of $Eu_{1-x}Y_xMnO_3$, the ferroelectric component points along the a direction. This would be compatible with a spiral vector along c (i.e., the spins rotating in the ab plane). The homogeneous canting of this helicoidal spin structure out of the ab plane could then generate the observed ferromagnetic moment along c.

V. CONCLUSION

In summary, we have characterized poly- and single-crystalline samples of the system $Eu_{1-x}Y_xMnO_3$ by means of structural, magnetic, thermodynamic, and dielectric measurements. In comparison with recently published results for the pure rare-earth systems we constructed a (T,x)-phase diagram for compositions $x \leqslant 0.5$. The ground state of $Eu_{1-x}Y_xMnO_3$ changes from a canted A-type AFM without long-range polar order for concentrations $x < 0.15$ towards a presumably spiral magnetic structure coexisting with a ferroelectric component for $x \geqslant 0.3$. For these higher Y concentrations the orientation of the ferroelectric component changes spontaneously from the c axis at higher temperatures towards the a axis for low temperatures. The regime with $P \| c$ increases with increasing Y concentration. In this sense $Eu_{1-x}Y_xMnO_3$ resembles the development of the ferroelectric orientation with decreasing ionic A-site radius as in the system $Tb_{1-x}Gd_xMnO_3$.[34] Hence, all essential magnetoelectric properties existing in the pure rare-earth compounds $GdMnO_3$ and $TbMnO_3$ are reproduced. The influence of the magnetic rare earth seems to be restricted to the distortion of the magnetic structure connected with the magnetic A-site ordering at low temperatures. The modulation of the magnetic structure related to the onset of ferroelectricity is realized due to the Mn sublattice only. However, the contraction of the lattice with increasing x in $Eu_{1-x}Y_xMnO_3$ is less effective than estimated from the average ionic A-site radii in comparison to the pure rare-earth compounds, which points towards the importance of disorder effects. The latter may also influence the properties in the concentration range around $x \approx 0.2$, where a finite spontaneous magnetic moment and ferroelectricity coexist. Such a FM and FE ground state has not been found in the pure rare-earth compounds so far and deserves further study. Even so it is plausible to expect a spontaneously canted spiral, the details of the underlying magnetic structure are not yet verified, and high-resolution investigations of the spin and lattice structure (e.g., with x-ray or neutron experiments) in the system $Eu_{1-x}Y_xMnO_3$ are highly needed.

ACKNOWLEDGMENTS

This work was partly supported by the Bundesministerium für Bildung und Forschung (BMBF) via Grant No. VDI/EKM 13N6917-A, by the Deutsche Forschungsgemeinschaft via Sonderforschungsbereich SFB 484 (Augsburg), and by INTAS and Russian Foundation for Basic Researches Grants No. 04-02-16592, No. 06-02-17514, and No. 04-02-81046-Bel2004.

[1] M. Fiebig, J. Phys. D **38**, R123 (2005).
[2] J. Hemberger, P. Lunkenheimer, R. Fichtl, H.-A. Krug von Nidda, V. Tsurkan, and A. Loidl, Nature (London) **434**, 364 (2005); P. Lunkenheimer, R. Fichtl, J. Hemberger, V. Tsurkan, and A. Loidl, Phys. Rev. B **72**, 060103(R) (2005).
[3] S. Weber, P. Lunkenheimer, R. Fichtl, J. Hemberger, V. Tsurkan, and A. Loidl, Phys. Rev. Lett. **96**, 157202 (2006).
[4] G. Lawes, A. B. Harris, T. Kimura, N. Rogado, R. J. Cava, A. Aharony, O. Entin-Wohlman, T. Yildirim, M. Kenzelmann, and C. Broholm, Phys. Rev. Lett. **95**, 087205 (2005).
[5] T. Lottermoser, T. Lonkai, U. Amann, D. Hohlwein, J. Ihringer, and M. Fiebig, Nature (London) **430**, 514 (2004).
[6] M. Fiebig, T. Lottermoser, D. Frohlich, A. V. Goitsev, and R. V. Pisarev, Nature (London) **419**, 818 (2002).
[7] N. Hur, S. Park, P. A. Sharma, J. S. Ahn, S. Guha, and S. W. Cheong, Nature (London) **429**, 392 (2004).
[8] T. Kimura, T. Goto, H. Shintani, K. Ishizaka, T. Arima, and Y. Tokura, Nature (London) **426**, 55 (2003).
[9] T. Goto, T. Kimura, G. Lawes, A. P. Ramirez, and Y. Tokura, Phys. Rev. Lett. **92**, 257201 (2004).
[10] T. Kimura, G. Lawes, T. Goto, Y. Tokura, and A. P. Ramirez, Phys. Rev. B **71**, 224425 (2005).
[11] I. A. Sergienko and E. Dagotto, Phys. Rev. B **73**, 094434 (2006).
[12] H. Katsura, N. Nagaosa, and A. V. Balatsky, Phys. Rev. Lett. **95**, 057205 (2005).
[13] C. Ederer and N. A. Spaldin, Phys. Rev. B **74**, 020401(R) (2006).
[14] J. Hemberger, S. Lobina, H.-A. Krug von Nidda, N. Tristan, V. Y. Ivanov, A. A. Mukhin, A. M. Balbashov, and A. Loidl, Phys. Rev. B **70**, 024414 (2004).
[15] T. Kimura, S. Ishihara, H. Shintani, T. Arima, K. T. Takahashi, K. Ishizaka, and Y. Tokura, Phys. Rev. B **68**, 060403(R) (2003).
[16] S. Quezel, F. Tcheou, J. Rossat-Mignod, G. Quezel, and E. Roudaut, Physica B & C **86**, 916 (1977).
[17] M. Kenzelmann, A. B. Harris, S. Jonas, C. Broholm, J. Schefer, S. B. Kim, C. L. Zhang, S. W. Cheong, O. P. Vajk, and J. W. Lynn, Phys. Rev. Lett. **95**, 087206 (2005).
[18] M. Mostovoy, Phys. Rev. Lett. **96**, 067601 (2006).
[19] T. Arima, T. Goto, Y. Yamasaki, S. Miyasaka, K. Ishii, M. Tsubota, T. Inami, Y. Murakami, and Y. Tokura, Phys. Rev. B **72**, 100102(R) (2005).
[20] N. Aliouane, D. N. Argyriou, J. Strempfer, I. Zegkinoglou, S. Landsgesell, and M. v. Zimmermann, Phys. Rev. B **73**, 020102(R) (2006).
[21] A. Pimenov, A. A. Mukhin, V. Y. Ivanov, V. D. Travkin, A. M. Balbashov, and A. Loidl, Nat. Phys. **2**, 97 (2006); A. Pimenov, T. Rudolf, F. Mayr, A. Loidl, A. A. Mukhin, and A. M. Balbashov, Phys. Rev. B **74**, 100403(R) (2006).
[22] H. Katsura, A. V. Balatsky, and N. Nagaosa, cond-mat/0602547, Phys. Rev. Lett. (to be published).
[23] N. A. Hill and A. Filippetti, J. Magn. Magn. Mater. **242**, 976 (1998).
[24] J. Baier, D. Meier, K. Berggold, J. Hemberger, A. Balbashov, J.

A. Mydosh, and T. Lorenz, Phys. Rev. B **73**, 100402(R) (2006).
[25] J. Hemberger, A. Krimmel, T. Kurz, H.-A. Krug von Nidda, V. Y. Ivanov, A. A. Mukhin, A. M. Balbashov, and A. Loidl, Phys. Rev. B **66**, 094410 (2002).
[26] R. Feyerherm, E. Dudzik, N. Aliouane, and D. N. Argyriou, Phys. Rev. B **73**, 180401(R) (2006).
[27] V. Y. Ivanov, A. A. Mukhin, V. D. Travkin, A. S. Prokhorov, A. M. Kadomtseva, Y. F. Popov, G. P. Vorob'ev, K. I. Kamilov, and A. M. Balbashov, Phys. Status Solidi B **243**, 107 (2006).
[28] A. M. Balbashov, S. G. Karabashev, Y. M. Mukovskiy, and S. A. Zverkov, J. Cryst. Growth **67**, 365 (1996).
[29] K. Noda, M. Akaki, T. Kikuchi, D. Akahoshi, and H. Kuwahara, J. Appl. Phys. **99**, 08S905 (2006).
[30] K. Taylor and M. Darby, *Physics of Rare Earth Solids* (Chapman and Hall Ltd., London, 1972).
[31] A. Herpin, *Theorie de Magnetism* (Presses Universitaires de France, Paris, 1968).
[32] I. Solovyev, N. Hamada, and K. Terakura, Phys. Rev. Lett. **76**, 4825 (1996).
[33] V. Skumryev, F. Ott, J. M. D. Coey, A. Anane, J.-P. Renard, L. Pinsard-Gaudart, and A. Revcolevschi, Eur. Phys. J. B **11**, 401 (1999).
[34] T. Goto, Y. Yamasaki, H. Watanabe, T. Kimura, and Y. Tokura, Phys. Rev. B **72**, 220403(R) (2005).